Hydroxysafflor Yellow A ameliorates adenomyosis by improving IDH1-autophagy-EMT

Xinran Li[1], Zhou Xu [1], Liwei Wang[2], Xintong Li[1], Xuefeng Wu[2], Xudong Wu[2], Hao Hong[1], Yan Shen[1,2]*, Ronghui Du[1]*

[1] State Key Laboratory of Pharmaceutical Biotechnology, Jiangsu Key Laboratory of Molecular Medicine, Medical School, Nanjing University, Nanjing 210093, China

[2] State Key Laboratory of Pharmaceutical Biotechnology, School of Life Sciences, Nanjing University, Nanjing 210023, China

***Correspondence:** shenyan@nju.edu.cn **(**Yan Shen**);** rhdu@nju.edu.cn (Ronghui Du)

Abstract

Background and Purpose:

Adenomyosis causes pain, abnormal bleeding, and infertility. Epithelial-mesenchymal transition (EMT) plays a critical role in the pathogenesis of adenomyosis. Current therapies are mainly hormone-dependent and their termination led to aggravations. To develop novel pharmacological treatment is necessary. Safflower was widely used to treat gynecological disease in China, the effect of hydroxysafflower yellow A (HSYA) that is the major active component of Safflower on adenomyosis remains unclear. We investigated whether HSYA ameliorates adenomyosis, and further revealed its potential target and mechanisms.

Experimental Approach:

Adenomyosis was induced in female ICR mice by oral administration of tamoxifen on days 2-5 after birth. At the 16th week, HSYA were administrated for 3 weeks. Adenomyosis development, autophagy activity, and involved mechanisms were analyzed using HE and Masson staining, western blotting, immunofluorescence, and RNA-sequencing. Furthermore, network pharmacology and molecular docking were applied to assess the potential target of HSYA.

Key Results:

HSYA ameliorates adenomyosis via promoting autophagy and ameliorating the activation of PI3K-AKT-mTOR. Isocitrate dehydrogenase1(IDH1) was found to be the potential target of HSYA. After IDH1 was knocked down by si-RNA, autophagy was activated, and EMT was attenuated via inhibiting PI3K-AKT-mTOR by HSYA.

Conclusions and Implications:

HSYA significantly ameliorates adenomyosis, and IDH1-autophagy-EMT plays an important role in the progress of adenomyosis. It will shed new light on a potential novel therapeutic strategy for adenomyosis.

Key words： adenomyosis； Hydroxysafflower yellow A (HSYA)； Isocitrate dehydrogenase1(IDH1); Epithelial-mesenchymal transition (EMT); Autophagy

1. Introduction

Adenomyosis is an estrogen-dependent gynecologic disease, characterized by the ectopic presence of endometrial islets within the myometrium(1), accompanied by dysmenorrhea, dyspareunia, pelvic pain, abnormal uterine bleeding (AUB), and

infertility(2). The incidence of adenomyosis significantly increases in recent years, and more women under the age of 40 suffer from the disease. Adenomyosis severely reduces the life quality of patients (3, 4). However, the etiology and pathogenesis of adenomyosis still remain unclearly clarified because there are many factors involved in the occurrence and development of adenomyosis. Epithelial-mesenchymal transition (EMT) that epithelial cells transdifferentiate into motile mesenchymal cells, was observed in the pathogenesis of adenomyosis(2, 5). Decreased E-cadherin expression and increased Vimentin and N-cadherin expression in the epithelial cells of adenomyosis(6) indicate that EMT contributes to the invasion and progression of adenomyotic lesions. EMT is essential in the development and wound healing and contributes to fibrosis and cancer progression. However, the reason that adenomyosis, a benign disease, behaves malignantly like tumors remains unclear. It has been reported that autophagy may be the node from the benign-to-malignant transition in EMT of several epithelial carcinomas(7). Autophagy serves as an intracellular recycling system(8), helps to remove misfolded proteins, damaged organelles, and lipid droplets to maintain cellular homeostasis by engulfing target structures into autophagosomes and fusing with lysosomes for degradation and enables cells to function properly. Accumulating evidence also indicate that aberrant autophagy occurs in the pathogenesis of endometriosis and adenomyosis(9, 10). However, the function of autophagy in adenomyosis remains controversial.

Current pharmacological therapy for adenomyosis mainly hormone-dependent including gonadotropin-releasing hormone agonists GnRHa, combined oral contraceptives, and progestins such as norethindrone acetate, medroxyprogesterone, and DNG, or levonorgestrel-releasing intrauterine system can improve the patient's life quality by relieving pain and bleeding(11). Women with symptomatic adenomyosis require life-long treatment. However, hormone therapy prevents conception. Termination of hormonal medications leads to recurrence. To develop novel pharmacological therapy is necessary. Traditional Chinese medicine is adept in treating gynecological diseases. In the present study, we evaluated whether hydroxysafflower yellow A (HSYA), the major active component of safflower which was widely treated gynecological disease (12), ameliorates adenomyosis.

Network pharmacology was performed to assess the compound-target combination and potential pathway of action of HSYA. Network pharmacology was first proposed in 2007 by Hopkins(13, 14) who combined drug-disease-target through network analysis which is different from one-target, one-drug, and one-disease. Network pharmacology match the therapeutic concept of traditional Chinese medicine, Chinese medicinal formulae act on multiple diseases or multiple targets. Network pharmacology provides instructive directions in exploring the mechanism of compound or traditional Chinese medicine in therapying diseases by analyzing the association between drugs and disease with a visible network. To clarify the prime target and the potential mechanisms of HSYA on adenomyosis, we further validated the results from network pharmacology by experiments.

In this study, we first evaluated the effect of HSYA on adenomyosis and EMT transition, that is the key pathological changes in adenomyosis. Then the key molecular mechanism in EMT induced by HSYA, was explored. Furthermore, potential action targets of HSYA were predicted by network pharmacology and validated by experiments.

2. Materials and methods

2.1. Cell culture

Ishikawa cells were purchased from ATCC and were cultured in RPMI 1640 supplemented with 10% fetal bovine serum (FBS; Gibco, CA, USA), streptomycin (100 μg/ml), and penicillin (100 μg/ml) in an incubator at 37℃ with 5% CO_2. Ishikawa cells were seeded in 24 wells until reached approximately 70% confluence. Then the complete medium was replaced with serum-free medium, and the cells were incubated with recombinant TGF-β1 (Pepro Tech, NJ, USA) and/or Hydroxysafflor yellow A (HSYA, MCE, Shanghai, China), which is dissolved in miliQ water.

2.2. Animal Experiments

ICR mice were purchased from Model Animal Research Center of Nanjing university (Nanjing, China). All mice were raised in a laboratory animal housing, 12 hours light/dark cycle conditions with acquiring clean water and food freely. Animal experimental protocols were approved by the Animal Care Committee of Nanjing University (NJU-ACUC) in accordance with European Directive 2010/63/EU. All female neonatal mice were born from 25 pregnant ICR mice. The mice were randomly divided into tamoxifen-treated and control groups. Tamoxifen-treated group were treated orally with 1 mg/kg tamoxifen (Sigma-Aldrich, St. Louis, MO) suspended in peanut oil/lecithin/condensed milk mixture (2:0.2:3 v/v, MCE, Shanghai, China)/day at a dose of 5 μl/g body weight on days 2 to 5 after birth (day of birth=day 1). On days 1 to 28 after birth mice were breastfed after birth. After 28 days, they were separated from the mother mice. At the 16th week after birth, mice were randomly divided into 5 groups (10/group): model (saline, ip), HSYA (2.5,5,10 mg/kg·d, i.p.), and celecoxib (6.5 mg/kg, Sigma-Aldrich, St. Louis, MO). Normal mice aged 16 weeks and model mice were given saline as control. After 3 weeks of treatment, both uterine horns were harvested to assess the severity of adenomyosis. Each uterine horn was divided into two portions. One portion was fixed in 4% paraformaldehyde and used paraffin embedded tissue. The other was frozen in liquid N_2 and stored at for -80℃.

2.3. H&E staining

After mice were sacrificed, uteruses were harvested, fixed with 4% paraformaldehyde (w/v, Sigma-Aldrich, St. Louis, MO) and paraffin embedded. Serial 4 μm sections were obtained from each paraffin-embedded tissue block. Sections were incubated at 60°C for 20 min, deparaffinized in xylene and rehydrated in a graded alcohol series. Sections were stained using the H&E Staining kit (Boster,Wuhan, China) according to the

manufacturer's instructions.

2.4. Masson trichrome staining

Masson's Trichrome staining (Solarbio, Beijing, China) were performed as follows: sections of the uterus were incubated at 60°C for 20 min, then deparaffinized in xylene and rehydrated in a graded alcohol series, immersed the sections in Bouin's solution at 37 °C overnight. The staining area were quantified with Image J software.

2.5. Immunofluorescence staining

Sections of the uteri were incubated at 60°C for 20 min, deparaffinized in xylene (Aladdin, Shanghai, China), and rehydrated in a graded alcohol series. Ishikawa cells grown on coverslips were fixed with 4% paraformaldehyde for 15 min. Sections and cell coverslips were permeabilized with 0.2% Triton-X 100(Sigma-Aldrich, St. Louis, MO) for 10 min, then blocked with 5% bovine serum albumin (BSA, Sigma-Aldrich, St. Louis, MO) for 1h at room temperature. Sections and cell coverslips were incubated with primary antibody overnight at 4°C overnight and incubated Alexa Fluor 594,488-conjugated secondary antibodies and DAPI for 1 hour at room temperature. Sections and cell coverslips were mounted with 100% glycerine (Aladdin, Shanghai, China), photographed with a Laser confocal microscope (OlympusFW3000). The staining area and protein positive spots were quantified by Image J software.

2.6. **Western blot analysis**

Total protein was extracted from Ishikawa cells or the uteri using the RIPA lysis buffer (Sangon Biotech, Shanghai, China) with containing 1% PMSF and 1% protease inhibitor cocktail (Sigma-Aldrich, St. Louis, MO). The proteins were separated on 10% SDS-PAGE gel, and transferred to PVDF membranes (Milipore, MA, USA), blocked with 5% nonfat milk for 2 hours in shaker at room temperature. Membranes were incubated with primary antibodies (Abcam, MA, USA) overnight at 4 ℃, then were washed with 1×TBST and incubated with secondary antibodies (Immunoway, TX, USA) for 2 hours in shaker at room temperature. Membranes were visualized via ECL electrochemiluminescence (Vazyme, Nanjing, China) and quantified with Image J software.

2.7. ELISA

The blood samples were collected from the mice and centrifuged at 3000 rpm for 15 min at 4℃ to acquire serum. TGF-β level in the serum was determined by Avidin–biotin complex–ELISA kits (Thermo Fisher, KS, USA) according to the manufacturer's instructions. The uteri were homogenized with PBS(PH=7.4) and centrifuged at 5000g for 20 min at 4℃, then supernatants were collected and store at -80℃ for further experiment. α-KG levels were determined by ELISA kit (Yifeixue, Nanjing, China) according to the manufacturer's instructions.

2.8. RNA sequencing

RNA sequencing (RNA-seq) was performed in Ishikawa cells incubated with or

without TGF-β. The length of the RNA fragments was detected using the Agilent 2100 Bioanalyzer Instruments (Agilent, USA). RNA-seq was performed with the PE150 sequencing strategy by the Illumina second-generation high-throughput sequencing platform. Trimmed reads were aligned by TopHat2, and transcript abundances and differences analyzed by cuffdiff.

2.9. Cell transfection

Ishikawa cells were transfected with siRNAs against IDH1 or LAMP using Universal Transfection Reagent (Hieff Trans, Shanghai, China) according to the manufacturer's instruction. The sequences of the siRNAs against IDH1 and LAMP1 were shown in Tab.1. Scramble were as negative control.

2.10. Collection of potential targets of HSYA

To identify the targets of HSYA, 3D-structure of HSYA was acquired from PubChem (https://pubchem.ncbi.nlm.nih.gov/), the structure was downloaded and saved in SDF format for further analysis. The potential targets were obtained though the PharmMapper (http://www.lilab-ecust.cn/pharmmapper/) by uploading 3D-structure of HSYA and Subsequently, the potential targets also obtained from ChEMBL (https://github.com/chembl) with the keyword "hydroxysafflor yellow A". Repetitive targets were removed.

2.11. Collection of potential targets of adenomyosis

Adenomyosis-related targets were retrieved from GeneCards (https://www.genecards.org/) and DisGeNET (https:// www. disgenet. Org) by querying keyword "Adenomyosis". After repetitive targets were removed, a database of adenomyosis-related targets was constructed.

2.12. Prediction of potential targets of adenomyosis for HSYA treatment

All the potential targets were input UniProt (https://www.uniprot.org/) with the species selected "homo sapiens" to acquire gene ID for the next analysis. The HSYA-related targets and adenomyosis-related targets databases imported into the Venny 2.1.0(https://bioinfogp.cnb.csic.es/tools/venny/index.html) to draw a Venn diagram. The common targets were retrieved as potential targets of HSYA for adenomyosis treatment.

2.13. Construction of protein-protein interaction (PPI) network

The potential targets were input the STRING database (https://cn.string-db.org/) with a high confidence (>0.7) and hide disconnected notes in the network to acquire a PPI network. The PPI network was download as TSV format and imported into the Cytoscape 3.8.0 software for visualization. The potential core targets were obtained by calculating the median values of "Degree", "Closeness", "Betweenness".

2.14. Gene ontology (GO) enrichment and Kyoto encyclopedia of genes and genomes (KEGG) pathway enrichment analysis

The potential targets of HSYA for adenomyosis treatment were enriched by the Database for Annotation, Visualization, and Integrated Discovery (DAVID) 6.8 (https://david.ncifcrf.gov/), and the threshold of $P < 0.05$ was set for key GO and KEGG pathway identification. The key pathways were visualized by online biological tools.

2.15. Construction of a compound-pathway-target network

The potential core targets and the key KEGG pathways were imported into Cytoscape 3.8.0 software to acquire a compound-pathway-target network. the network was visualized and analyzed via Cytoscape software.

2.16. Molecular docking analysis

The molecular structures of potential core targets were obtained from PubChem (https://pubchem.ncbi.nlm.nih.gov/). Autodock Vina was used for flexible docking and binding energy analysis. The 3D-docking plot of targets with HSYA was drawn to analysis the hydrogen bonding energy between key amino acid residues.

2.17. Statistical analysis

Quantitative data were presented as the mean ± SEM, and represent at least 3 independent experiments. SPSS 13.0 statistical software (SPSS Inc.) and GraphPad Prism 5.0 software were used for processing data. Unpaired t-test was performed for comparisons between two groups and One-way analysis of variance (ANOVA) test was performed for comparisons among multiple groups. A p value<0.05 was considered statistically significant.

3. Results

3.1. HSYA attenuated Tamoxifen-induced adenomyosis in mice.

The structure of HSYA was shown in Fig.1A. To assess the effect of HSYA on adenomyosis, neonatal mice were treated with Tamoxifen to induce adenomyosis and various doses of HSYA and celecoxib were administered from 16w to 19w (Fig.1B). Adenomyosis is characterized by the thickness increase of the uterus and penetration of the ectopic endometrium into the myometrium. As exhibited in Fig 1C, adenomyosis mice manifested abnormal myometrial structure that glands and stromal cells are observed in the myometrium. The depth of ectopic endometrial infiltration into the myometrium was graded using the criteria: Grade 0, none of the ectopic endometrium in the myometrium; Grade 1, the superficial myometrium penetration; Grade 2, the mid myometrium penetration; and Grade 3, beyond the mid myometrium penetration. Adenomyosis lesions were analyzed by Hematoxylin and eosin staining. The thickness of adenomyosis mice uteri and the invasion of the endometrium into myometrium were significantly attenuated by HSYA in a dose-dependent manner (Fig.1C, D). Fibrosis was detected by Masson's trichrome stain. Myometrial collagen expression in adenomyosis mice was dose-dependently decreased by HSYA, the effect of HSYA at the dose of 5 mg/kg and 10 mg/kg on the thickness and fibrosis of uteri were better than that in celecoxib, a COX-2 selective inhibitor which has been utilized as an anti-inflammatory medication (Fig.1C-E).

3.2. HSYA inhibited EMT in adenomyosis mice

Epithelial-mesenchymal transition (EMT) was involved in adenomyosis. To determine whether HSYA attenuated epithelial-mesenchymal transition (EMT), immunofluorescence of E-cadherin and Vimentin was performed in the uterus section of adenomyosis mice. The decrease of E-cadherin expression and the increase of N-cadherin and Vimentin which are hallmarks of EMT. As shown in Fig.2A, E-cadherin, the epithelial cell marker, was down-regulated, and Vimentin, the mesenchymal marker, was up-regulated in the endometrium in adenomyosis mice, suggesting that EMT occurred in adenomyosis mice. HSYA significantly reduced EMT while celecoxib had no remarkable effect (Fig.2A-C). Western blotting analysis further confirmed that HSYA dose-dependently attenuated EMT (Fig.2B, C). To further assess the effect of HSYA on EMT, TGF-β in the serum were determined by ELISA. Increased TGF-β levels in the serum of adenomyosis mice were dose-dependently suppressed by HSYA (Fig.2D). The amelioration of Celecoxib on EMT is little (Fig.2A-D). Furthermore, decrease of E-cadherin expression and increase of N-cadherin and Vimentin were also observed in Ishikawa cells treated with TGF-β at the concentrations of 3 ng/ml and 10 ng/ml for 24 h (Fig.2E, F). To find the right time of EMT progression and to investigate the molecular mechanism, we continue to evaluate the time-effect relationship of EMT induced by TGF-β in Ishikawa cells at 6,12, and 24h after the stimulation. The decrease in E-cadherin together with the increase in Vimentin and N-cadherin significantly were observed when Ishikawa cells were stimulated by TGF-β for 24h (Fig.2G, H). N-cadherin was significantly decreased, and Vimentin and N-cadherin were increased by HSYA in a dose-dependent manner (Fig.2I, J). Immunofluorescence staining confirmed that HSYA inhibited EMT induced by TGF-β in Ishikawa cells (Fig.2K, L).

3.3. HSYA induced autophagy via the PI3K-AKT signaling pathway in Ishikawa cells and adenomyosis mice

To understand the effect of HSYA on adenomyosis, transcriptome analysis was performed in Ishikawa cells with or without TGF-β (3 ng/ml) for 24h. 20 significantly enriched KEGG pathways were identified. These pathways involved the PI3K-AKT signaling pathway, ECM-receptor interaction, and TGF-β signaling pathway (Fig.3A). Western blots confirmed that the PI3K-AKT-mTOR pathway was activated in Ishikawa cells induced by TGF-β(3ng/ml) for 24 h, and HSYA inhibited the overactivation (Fig.3B, C). AKT/mTOR signaling pathway plays a key role in regulating autophagy which is closely related to the physiological activity of the uterus, thus the effect of HSYA on autophagy was evaluated. The ratio of LC3 I to LC3 II which are the marker of autophagy activation and P62, an indicator of autophagic protein degradation were examined. As shown in Fig.3D and Fig.3E, P62 increased and the ratio of LC3I to LC3II decreased after Ishikawa cells was co-incubated with TGF-β(3ng/ml), and HSYA decreased P62 protein level and increased the ratio of LC3I to LC3 II. We continued to evaluate whether HSYA effected on PI3K-AKT-mTOR pathway and autophagy in adenomyosis mice. p-PI3K, p-AKT, and p-mTOR were significantly activated in the uteri of adenomyosis mice and the over-activation was inhibited by HSYA which were

consistent with that in Ishikawa cells. Meanwhile, P62 decreased and the transition of LC3II increased in the uteri of adenomyosis mice (Fig.3F, G). The immunofluorescence images of LC3 and P62 in mouse uteri were consistent with that of western blots (Fig.3H, I). These results suggested that autophagy was upregulated by HSYA together with the inhibition of the PI3K-AKT-mTOR pathway.

3.4. HSYA promoted autophagic flux and improved EMT through the PI3K-AKT-mTOR signaling pathway in Ishikawa cells

To confirm whether the PI3K-AKT-mTOR pathway plays an important role in HSYA-induced autophagy regulation, the mTOR inhibitor rapamycin and autophagic flux inhibitor, Baf A1, were also incubated with Ishikawa cells. P62 was significantly increased and the ratio of LC3 I to LC3 II decreased, accompanying by the activation of p-PI3K, pAKT, and p-mTOR after Ishikawa cells were stimulated with TGF-β; HSYA, acting similarly to Rapa, enhanced autophagy and decreased the over-activating of PI3K-AKT-mTOR pathway (Fig.4A, B). Baf A1, the autophagic flux inhibitor, blocks the degradation of autophagosomes by inhibiting the fusion of autophagosomes with lysosomes, further inhibited autophagy induced by TGF-β, HSYA improved the suppression of autophagy. These data indicated that the PI3K-AKT-mTOR pathway was involved in the autophagy-regulation induced by HSYA (Fig.4C, D). To evaluate whether HSYA improves autophagy by inhibiting the degradation of autophagosomes or promoting autophagic flux, immunofluorescence was performed to detect the fusion of autophagy and lysosomes. As shown in Fig.4E, HSYA increased the co-localization of autophagy and lysosome. To confirm whether autophagic flux played a key role in the effect of HSYA on EMT, LAMP2 was knocked down in Ishikawa cell. The degradation of P62 and the transition of LC3I to LC3II were inhibited, and EMT increased after LAMP2 was knocked down. HSYA hardly effects on improving autophagy and decreasing EMT after LAMP2 was knocked down. It indicated that HSYA improved EMT via increasing autophagic flux (Fig.4F-I).

3.5. Compound-disease-target prediction based on network pharmacology

To explore the potential targets of HSYA for adenomyosis, network pharmacology is performed. A total of 449 targets were collected based on PharmMapper and ChEMBL, and 415 adenomyosis-related targets were collected from GeneCards and DisGeNET database. After standardizing with Uniprots, all targets are analyzed by Venn diagrams. A total of 36 overlapping targets were obtained, which were considered the potential targets of HSYA for adenomyosis treatment (Fig. 5A). To elucidate the potential mechanism by which HSYA therapies adenomyosis, the gene names of 36 HSYA anti-adenomyosis targets were imported into the STRING database to construct a PPI network. With high confidence (>0.7), the network containing 36 nodes and 46 edges was obtained.

To identify the core targets, the active compound-disease-target network was visualized using Cytoscape 3.8.0 according to the target degree. Darker colors and larger nodes represent greater degree values (Fig.5B). Potential targets were analyzed in the KEGG

enrichment using DAVID v6.8 and those potential targets were enriched in 59 pathways. Among the top 20 enriched pathways, 10 were associated with adenomyosis. To reveal the association between the potential core targets and pathways, 36 potential core targets and 10 disease-related KEGG pathways were imported into Cytoscape 3.8.0 software for visualization and acquired a component-target-pathway network. The yellow node represented HSYA, the green nodes represented potential core targets, and the blue nodes represented pathways, in which the larger size of the node implied a greater degree value. The potential core targets were enriched in three pathways which are related to the progression of adenomyosis (Fig.5C). The importance and criticality of nodes were reflected by Degree and Closeness, and the proximity among nodes was reflected by Betweenness. We screened the nodes in which these three values are higher than the median (Degree>14, Closeness>0.5078, Betweenness>0.004143) as the core potential targets. A total of 10 potential core targets were obtained including AKT1, MMP2, CAT, EGFR, NOS3, ESR2, MMP9, RHOA, IDH1, and MMP3. To further screen the potential targets of HSYA for adenomyosis therapy, we used Autodock Vina software for molecular docking to validate the binding modes of targets with HSYA. The binding energies were calculated to evaluate the stabilization of binding between the component and the protein. The binding energies ≤-7 kJ·mol-1 indicated that the component had a good binding activity with the protein. The binding affinities were shown in Table 2, there were 7 targets that binding affinities ≤-7 kJ·mol-1, including AKT1, MMP2, CAT, EGFR, NOS3, IDH1, and ESR2. The important docking results of the targets with HSYA are shown in Fig.5D. To confirm the docking results, western blots of AKT1, NOS3, EGFR, and IDH1 were performed. NOS3, AKT1, and IDH1 were increased and EGFR was decreased in uteri of adenomyosis mice (Fig.5E, F).

3.6. IDH1 was inhibited by HSYA in the uteri of adenomyosis mice and Ishikawa cells induced by TGF-β

To evaluate the effect of HSYA on isocitrate dehydrogenase1 (IDH1), western blots were utilized to detect IDH1 expressions in the uteri of adenomyosis mice. IDH1 was up-regulated in adenomyosis mice uteri, and HSYA attenuated the over-expression of IDH1(Fig.6A, B). Immunofluorescence results were consistent with that of western blots (Fig.6C). IDH1 is a critical metabolic enzyme that catalyzes the oxidative decarboxylation of isocitrate to alpha-ketoglutarate (α-KG). To confirm the effect of HSYA on IDH1, α-KG in mice uterus was determined by ELISA. Overexpressed α-KG in adenomyosis mice was decreased by HSYA in a dose-dependent manner (Fig.6E). IDH1 levels increased in Ishikawa cells stimulated by TGF-β, and HSYA dose-dependently reduced the over-expression of IDH1. These results suggested that IDH1 was the potential target of HSYA (Fig.6F-I).

3.7. HSYA significantly inhibited EMT by promoting autophagy after IDH1 was knocked down by siRNA

To confirm whether IDH1 plays an important role in EMT, IDH1 was knocked down by siRNA in Ishikawa cells. P62 was decreased and the transition from LC3 I to LC3 II was increased in Ishikawa cells after IDH1 was knocked down by siRNA, indicating

that autophagic influx was enhanced after IDH1 was knocked down, and autophagic flux was improved by HSYA(Fig7A-D). Western Blots further indicated that E-cadherin was up-regulated and N-cadherin was downregulated in Ishikawa cells after IDH1 was knocked down (Fig.7E, F). Immunofluorescence images confirmed after IDH1 was knocked down, E-cadherin increased, and vimentin decreased (Fig.7G), indicating that EMT transition was suppressed after IDH1 was knockdown. The inhibition of EMT induced by HSYA was further enhanced after IDH1 was knockdown, in particular, Vimentin level was significantly decreased (Fig.7H, I). After IDH1 was knocked down, p-PI3K, p-AKT, and p-mTOR were inhibited, and HSYA medication did not further inhibit PI3K-AKT-mTOR pathway, confirming that IDH1 was the potential target of HSYA (Fig.7J-M).

4. Discussion

In the present study, our data firstly indicated that hydroxy safflower yellow A(HSYA), ameliorated adenomyosis. IDH1 was found that it was the potential therapeutic target of HSYA. It is potential to solve symptoms recur after withdrawal of hormone therapy for adenomyosis.

To reveal the pathophysiological mechanism of adenomyosis and evaluate the effect of HSYA, a tamoxifen-induced adenomyosis murine model was firstly utilized(15). EMT and ultimate fibrosis play a critical role in the pathogenesis of adenomyosis, and adenomyosis is characterized by the presence of endometrial glands and stroma in the myometrium. The uteri of tamoxifen-induced adenomyosis mice exhibited an abnormal structure in the myometrium, together with losing cell polarity and cell-cell adhesion, endometrial glands, and stroma presenting in the myometrium. In the uteri of adenomyosis mice, fibrosis and its key driving factor TGF-β increased. These results indicated that tamoxifen-induced adenomyosis mice are successfully established in the present study. The experimental adenomyosis mice model is no surgery required, with a high successful rate and a little inter-individual variation. HSYA improved the abnormal structure. Our data indicated that HSYA ameliorated adenomyosis in mice for the first time. Jiang et al also found that HSYA suppressed EMT in A549 and H1299 cells(16).

To evaluate the pathogenesis of EMT in adenomyosis, RNA-seq, and bioinformatics were used for the analysis and annotation of differential gene expression (DEGs) of EMT in Ishikawa cells in the absence or presence of TGF-β. The PI3K-AKT signaling pathway was activated after Ishikawa cells were stimulated with TGF-β. HSYA inhibited the over-activation of the PI3K-AKT-mTOR pathway. PI3K-AKT-mTOR was a classical pathway regulating autophagy initiation, and it was involved in the process of many diseases including neurodegeneration, cancer and et al (17). Our data indicated that HSYA promoted the conversion of LC3I to LC3II, and increased the degradation of P62. Yang et al found that HSYA protected brain microvascular endothelial cells (BMECs) by inhibiting autophagy(18). Other researchers' work suggested that HSYA induced an autophagic response in THP-1 macrophage via the

PI3K/AKT/mTOR signaling pathway (19, 20). Our data firstly demonstrated that HSYA inhibited EMT by promoting autophagy in Ishikawa cells and experimental adenomyosis mice. Autophagosome-lysosome fusion is necessary to maintain autophagic flux that constitutes late steps in the autophagic process(21). Our data demonstrated that HSYA promotes the fusion of autophagosomes and lysosomes in Ishikawa cells. LAMP are estimated to contribute to about 50% of all proteins of the lysosome membrane(22).After LAMP2 was knocked down via siRNA, autophagy was inhibited and EMT increased. In adenomyosis mice and Ishikawa cells, we observed that HSYA inhibited EMT by promoting the formation of autophagic flux. Jiang et al found that HSYA inhibited EMT transition in lung cancer cells(16).

Despite our data demonstrating that HSYA effected on AKT-autophagy-EMT, the precise target of HSYA on adenomyosis remains unclear. In complex diseases, interventions at a single target do not work well though 'one drug for one target for one disease' has influenced drug-discovery strategy for many years. Yıldırım et al. proposed to apply network to analyze drugs and drug targets(23). Network pharmacology was used for predicting targets of traditional Chinese medicine in diseases to elucidate the pharmacological mechanisms in recent decades (24, 25). Potential targets of HSYA for adenomyosis were predicted via network pharmacology. PI3K-AKT pathway was significantly enriched, suggesting that this pathway played a key role in adenomyosis progression, it is consistent with the results of RNA-seq. Hu's data also indicated that the proliferative activity of endometrial cells was activated by the PI3K-AKT pathway in adenomyosis(26). Core potential targets were further identified by PPI analysis and validated them using molecular docking analysis. The top5 protein are AKT1, NOS3, MMP2, EGFR and IDH1. MMP-2, together with MMP-3 and MMP-9, known as the gelatinases, are the main contributors to the ECM's degradation during tumor invasion(27). AKT1, NOS3, and IDH1 were upregulated and EGFR was downregulated in experimental adenomyosis mice. Increased NOS3 expression is associated with dysmenorrhea and high NO production by ectopic endothelium(28). EGFR is a receptor tyrosine kinase binding ligand of the EGF family and activates several signaling cascades such as RAS-RAF-MEK-ERK, PI3 kinase-AKT, PLCgamma-PKC, and STATs modules. Some studies were shown that the activation of the EGF/EGFR signaling pathway eventually leads to epithelial-mesenchymal transition in cancer(29). Herein, we validated AKT1, NOS3, EGFR, and IDH1 in experimental adenomyosis mice by western blot. Our data confirmed that Akt1, NOS3 and IDH1 were upregulated in the uterus of adenomyosis mice. NOS3 is also named endothelial NOS. Hatazawa et al observed that endothelial NOS was moderately positive in adenomyosis patients(30). Wu et al also reported that the expressions of eNOS were significantly higher in adenomyosis than that in normal endometrium(31). These data indicated that the results of network pharmacology combined with docking to predict targets are credible.

Isocitrate dehydrogenases (IDHs) are critical metabolic enzymes in the TCA cycle(32). We focus on evaluating the effect of IDH1 on adenomyosis. IDH1 was upregulated in experimental mice's uteri and Ishikawa cells stimulated with TGF-β. After IDH1 was

knocked down in Ishikawa cells, the PI3K-AKT-mTOR pathway was down-regulated and autophagy was enhanced. Mallette et al also reported that the TCA cycle is linked to the canonical PI3K/AKT pathway(33). IDH1/2 normally catalyzes the oxidative decarboxylation of isocitrate into a-ketoglutarate (α-KG) (34). To evaluate the effect of HSYA on IDH1, α-KG in the uterus of mice was determined by ELISA. HSYA dose-dependently decreased the level of α-KG in adenomyosis mice, which is consistent with the down-regulation of IDH1 expression.

Different from our results, Yalaza et al found that IDH1 expression at the mRNA level was decreased in adenomyosis patients(35). The credibility is worth considering because observations only limited to RNA levels and there is significant patient-to-patient variation. Our data at the protein level are from Ishikawa cells and experimental adenomyosis mice with relatively small individual differences, it is more creditable. To further confirm the role of IDH1 in adenomyosis, we continued to evaluate EMT by knocking down IDH1 in Ishikawa cells. EMT was decreased after IDH1 was knocked down. Grassian et al found that normal epithelial morphology was reversibly disrupted through EMT after IDH is mutant (36), which are consistent with our results that IDH1 is important to maintain the epithelial morphology.

In the present study, we found that HSYA ameliorated adenomyosis, IDH1-Autophagy-EMT played a critical role in adenomyosis, and IDH1 is the potential target of HSYA.

CRediT authorship contribution statement

Ronghui Du and Xinran Li conceived the study and wrote the paper. Xu Zhou, Liwei Wang, and Xintong Li, Xuefeng Wu, Xudong Wu and Yan Shen performed the experiments. Xintong Li, Yan Shen, Hao Hong and Ronghui Du reviewed and edited the manuscript. All authors have read and approved the final version of the manuscript submitted for publication.

Declaration of competing interest

The authors declare that there have no conflicts of interest.

Funding

This work was financially supported by the National Natural Science Foundation of China (No.81673430, 81974504 and 82073910) and Specific grant of State Key Laboratory of Pharmaceutical Biotechnology (No. 20221212).

Reference

1. Benagiano G, Habiba M, Brosens I. The pathophysiology of uterine adenomyosis: an update. Fertil Steril. 2012;98(3):572-579.
2. Guo SW. The Pathogenesis of Adenomyosis vis-a-vis Endometriosis. J Clin Med. 2020;9(2).
3. Chapron C, Vannuccini S, Santulli P, Abrao MS, Carmona F, Fraser IS, Gordts S, Guo SW, Just PA, Noel JC, Pistofidis G, Van den Bosch T, Petraglia F. Diagnosing adenomyosis: an

integrated clinical and imaging approach. Hum Reprod Update. 2020;26(3):392-411.
4. Horton J, Sterrenburg M, Lane S, Maheshwari A, Li TC, Cheong Y. Reproductive, obstetric, and perinatal outcomes of women with adenomyosis and endometriosis: a systematic review and meta-analysis. Hum Reprod Update. 2019;25(5):592-632.
5. Hu Y, Yuan M, Cheng L, Wang G. Extracellular vesicles contribute to EMT in adenomyosis by inducing macrophage polarizationdagger. Biol Reprod. 2023;108(4):584-596.
6. Jin Z, Wu X, Liu H, Xu C. Celecoxib, a selective COX-2 inhibitor, markedly reduced the severity of tamoxifen-induced adenomyosis in a murine model. Exp Ther Med. 2020;19(5):3289-3299.
7. Su Z, Yang Z, Xu Y, Chen Y, Yu Q. Apoptosis, autophagy, necroptosis, and cancer metastasis. Mol Cancer. 2015;14:48.
8. Zhao YG, Codogno P, Zhang H. Machinery, regulation and pathophysiological implications of autophagosome maturation. Nat Rev Mol Cell Biol. 2021;22(11):733-750.
9. Huang Y, Zhao Y, Liu H, Yang Y, Cheng L, Deng X, Chao L. Decreased expression of GRIM-19 induces autophagy through the AMPK/ULK1 signaling pathway during adenomyosisdagger. Biol Reprod. 2022;107(4):956-966.
10. Cacciottola L, Camboni A, Cernogoraz A, Donnez J, Dolmans MM. Role of apoptosis and autophagy in ovarian follicle pool decline in children and women diagnosed with benign or malignant extra-ovarian conditions. Hum Reprod. 2023;38(1):75-88.
11. Vannuccini S, Petraglia F. Recent advances in understanding and managing adenomyosis. F1000Res. 2019;8.
12. Zhou X, Tang L, Xu Y, Zhou G, Wang Z. Towards a better understanding of medicinal uses of Carthamus tinctorius L. in traditional Chinese medicine: a phytochemical and pharmacological review. J Ethnopharmacol. 2014;151(1):27-43.
13. Hopkins AL. Network pharmacology. Nat Biotechnol. 2007;25(10):1110-1111.
14. Hopkins AL. Network pharmacology: the next paradigm in drug discovery. Nat Chem Biol. 2008;4(11):682-690.
15. Mehasseb MK, Bell SC, Habiba MA. Neonatal administration of tamoxifen causes disruption of myometrial development but not adenomyosis in the C57/BL6J mouse. Reproduction. 2010;139(6):1067-1075.
16. Jiang M, Zhou LY, Xu N, An Q. Hydroxysafflor yellow A inhibited lipopolysaccharide-induced non-small cell lung cancer cell proliferation, migration, and invasion by suppressing the PI3K/AKT/mTOR and ERK/MAPK signaling pathways. Thorac Cancer. 2019;10(6):1319-1333.
17. Song M, Bode AM, Dong Z, Lee MH. AKT as a Therapeutic Target for Cancer. Cancer Res. 2019;79(6):1019-1031.
18. Yang G, Wang N, Seto SW, Chang D, Liang H. Hydroxysafflor yellow a protects brain microvascular endothelial cells against oxygen glucose deprivation/reoxygenation injury: Involvement of inhibiting autophagy via class I PI3K/Akt/mTOR signaling pathway. Brain Res Bull. 2018;140:243-257.
19. Jia-Xi L, Chun-Xia Z, Ying H, Meng-Han Z, Ya-Nan W, Yue-Xin Q, Jing Y, Wen-Zhi Y, Miao-Miao J, De-An G. Application of multiple chemical and biological approaches for quality assessment of Carthamus tinctorius L. (safflower) by determining both the primary and secondary metabolites. Phytomedicine. 2019;58:152826.

20. Jiang Y, Kou J, Han X, Li X, Zhong Z, Liu Z, Zheng Y, Tian Y, Yang L. ROS-Dependent Activation of Autophagy through the PI3K/Akt/mTOR Pathway Is Induced by Hydroxysafflor Yellow A-Sonodynamic Therapy in THP-1 Macrophages. Oxid Med Cell Longev. 2017;2017:8519169.
21. Mauthe M, Orhon I, Rocchi C, Zhou X, Luhr M, Hijlkema KJ, Coppes RP, Engedal N, Mari M, Reggiori F. Chloroquine inhibits autophagic flux by decreasing autophagosome-lysosome fusion. Autophagy. 2018;14(8):1435-1455.
22. Eskelinen EL. Roles of LAMP-1 and LAMP-2 in lysosome biogenesis and autophagy. Mol Aspects Med. 2006;27(5-6):495-502.
23. Yildirim MA, Goh KI, Cusick ME, Barabasi AL, Vidal M. Drug-target network. Nat Biotechnol. 2007;25(10):1119-1126.
24. Pan HD, Yao XJ, Wang WY, Lau HY, Liu L. Network pharmacological approach for elucidating the mechanisms of traditional Chinese medicine in treating COVID-19 patients. Pharmacol Res. 2020;159:105043.
25. Zhu J, Jin Z, Yang L, Zhao C, Hu J, Chen J, Han Y, Yu P, Luo J, Kong L, Zhang C. Ginkgolide B targets and inhibits creatine kinase B to regulate the CCT/TRiC-SK1 axis and exerts pro-angiogenic activity in middle cerebral artery occlusion mice. Pharmacol Res. 2022;180:106240.
26. Xu XY, Zhang J, Qi YH, Kong M, Liu SA, Hu JJ. Linc-ROR promotes endometrial cell proliferation by activating the PI3K-Akt pathway. Eur Rev Med Pharmacol Sci. 2018;22(8):2218-2225.
27. Gobin E, Bagwell K, Wagner J, Mysona D, Sandirasegarane S, Smith N, Bai S, Sharma A, Schleifer R, She JX. A pan-cancer perspective of matrix metalloproteases (MMP) gene expression profile and their diagnostic/prognostic potential. BMC Cancer. 2019;19(1):581.
28. Oh NJ, Ryu KY, Jung CN, Yi SY, Kim SR. Expression of endothelial nitric oxide synthase in the uterus of patients with leiomyoma or adenomyosis. J Obstet Gynaecol Res. 2013;39(2):536-542.
29. Li Q, Bao W, Fan Q, Shi WJ, Li ZN, Xu Y, Wu D. Epidermal growth factor receptor kinase substrate 8 promotes the metastasis of cervical cancer via the epithelial-mesenchymal transition. Mol Med Rep. 2016;14(4):3220-3228.
30. Hatazawa J, Ota H, Murata M, Igarashi S, Tanaka T. Localization of endothelial nitric oxide synthase messenger ribonucleic acid by in situ hybridization in ectopic endometrial tissue in patients with adenomyosis. Reprod Fertil Dev. 2000;12(5-6):283-287.
31. Wu MY, Chao KH, Yang JH, Lee TH, Yang YS, Ho HN. Nitric oxide synthesis is increased in the endometrial tissue of women with endometriosis. Hum Reprod. 2003;18(12):2668-2671.
32. Liu J, Peng Y, Shi L, Wan L, Inuzuka H, Long J, Guo J, Zhang J, Yuan M, Zhang S, Wang X, Gao J, Dai X, Furumoto S, Jia L, Pandolfi PP, Asara JM, Kaelin WG, Jr., Liu J, Wei W. Skp2 dictates cell cycle-dependent metabolic oscillation between glycolysis and TCA cycle. Cell Res. 2021;31(1):80-93.
33. Carbonneau M, L MG, Lalonde ME, Germain MA, Motorina A, Guiot MC, Secco B, Vincent EE, Tumber A, Hulea L, Bergeman J, Oppermann U, Jones RG, Laplante M, Topisirovic I, Petrecca K, Huot ME, Mallette FA. The oncometabolite 2-hydroxyglutarate activates the mTOR signalling pathway. Nat Commun. 2016;7:12700.

34. Liu S, Abboud MI, John T, Mikhailov V, Hvinden I, Walsby-Tickle J, Liu X, Pettinati I, Cadoux-Hudson T, McCullagh JSO, Schofield CJ. Roles of metal ions in the selective inhibition of oncogenic variants of isocitrate dehydrogenase 1. Commun Biol. 2021;4(1):1243.
35. Yalaza C, Canacankatan N, Gurses I, Aytan H, Tasdelen B. Altered VEGF, Bcl-2 and IDH1 expression in patients with adenomyosis. Arch Gynecol Obstet. 2020;302(5):1221-1227.
36. Grassian AR, Lin F, Barrett R, Liu Y, Jiang W, Korpal M, Astley H, Gitterman D, Henley T, Howes R, Levell J, Korn JM, Pagliarini R. Isocitrate dehydrogenase (IDH) mutations promote a reversible ZEB1/microRNA (miR)-200-dependent epithelial-mesenchymal transition (EMT). J Biol Chem. 2012;287(50):42180-42194.

Tab 1 Primers of Si-RNA.

Gene	sense	antisense
si-IDH1	GCAUAAUGUUGGCGUCAAATT	UUUGACGCCAACAUUAUGCTT
si-LAMP2	GCAAAAUGGCAGAUGAAUUTT	AAUUCAUCUGCCAUUUUGCTT
scrambled siRNA	UUCUCCGAACGUGUCACGUTT	ACGUGACACGUUCGGAGAATT

Tab 2. Molecular docking binding energy of TOP10 potential core target

No.	Gene ID	Gene Name	Protein name	Affinity
1	207	AKT1	AKT serine/threonine kinase 1	-9.6
2	4846	NOS3	nitric oxide synthase 3	-9
3	4313	MMP2	matrix metallopeptidase 2	-8.5
4	3417	IDH1	isocitrate dehydrogenase (NADP(+)) 1	-8.2
5	1956	EGFR	epidermal growth factor receptor	-8.2
6	847	CAT	catalase	-7.2
7	2100	ESR2	estrogen receptor 2	-7.1
8	4314	MMP3	matrix metallopeptidase 3	-6.8
9	4318	MMP9	matrix metallopeptidase 9	-6.7
10	387	RHOA	ras homolog family member A	-6.7

Figures

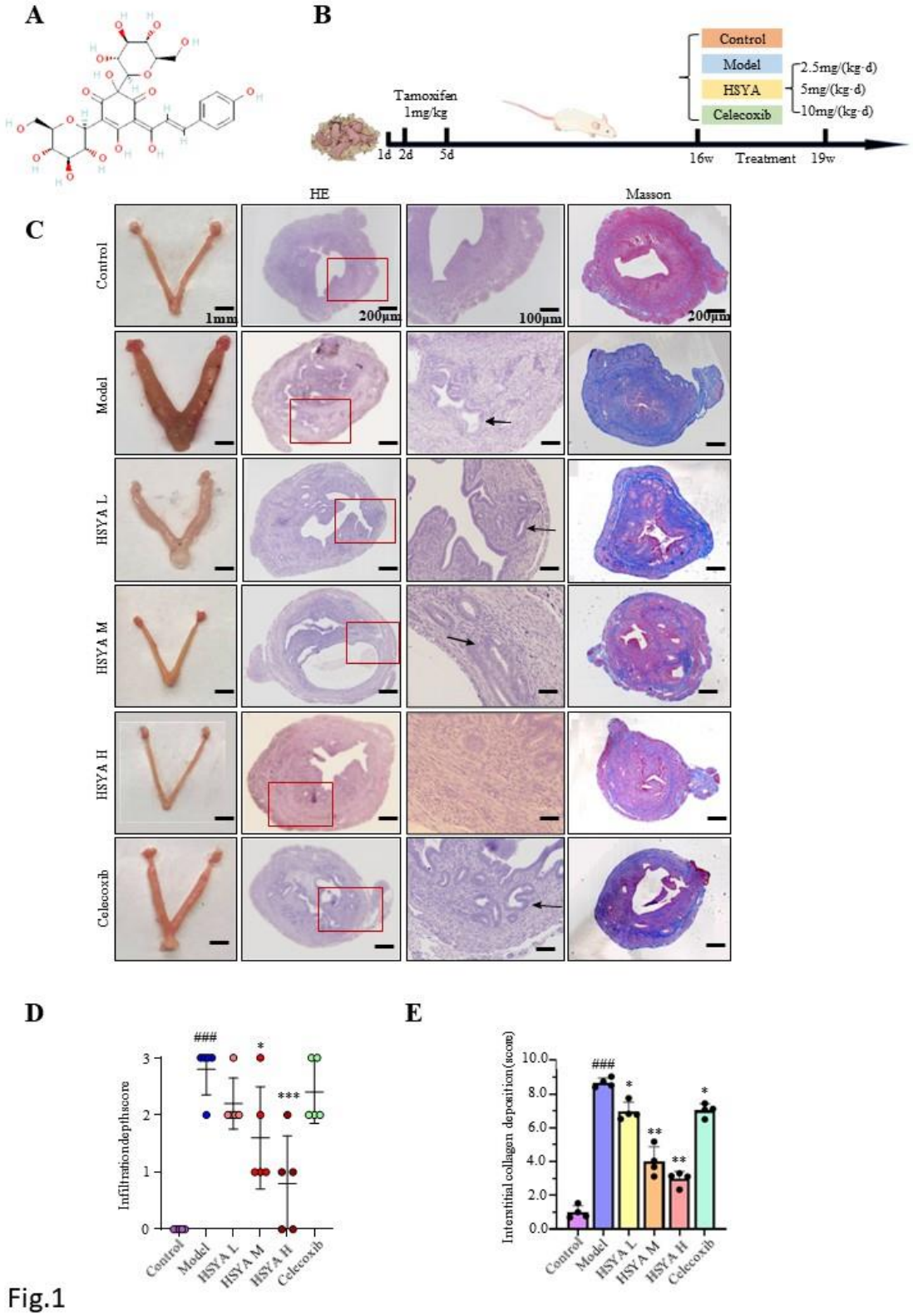

Fig.1

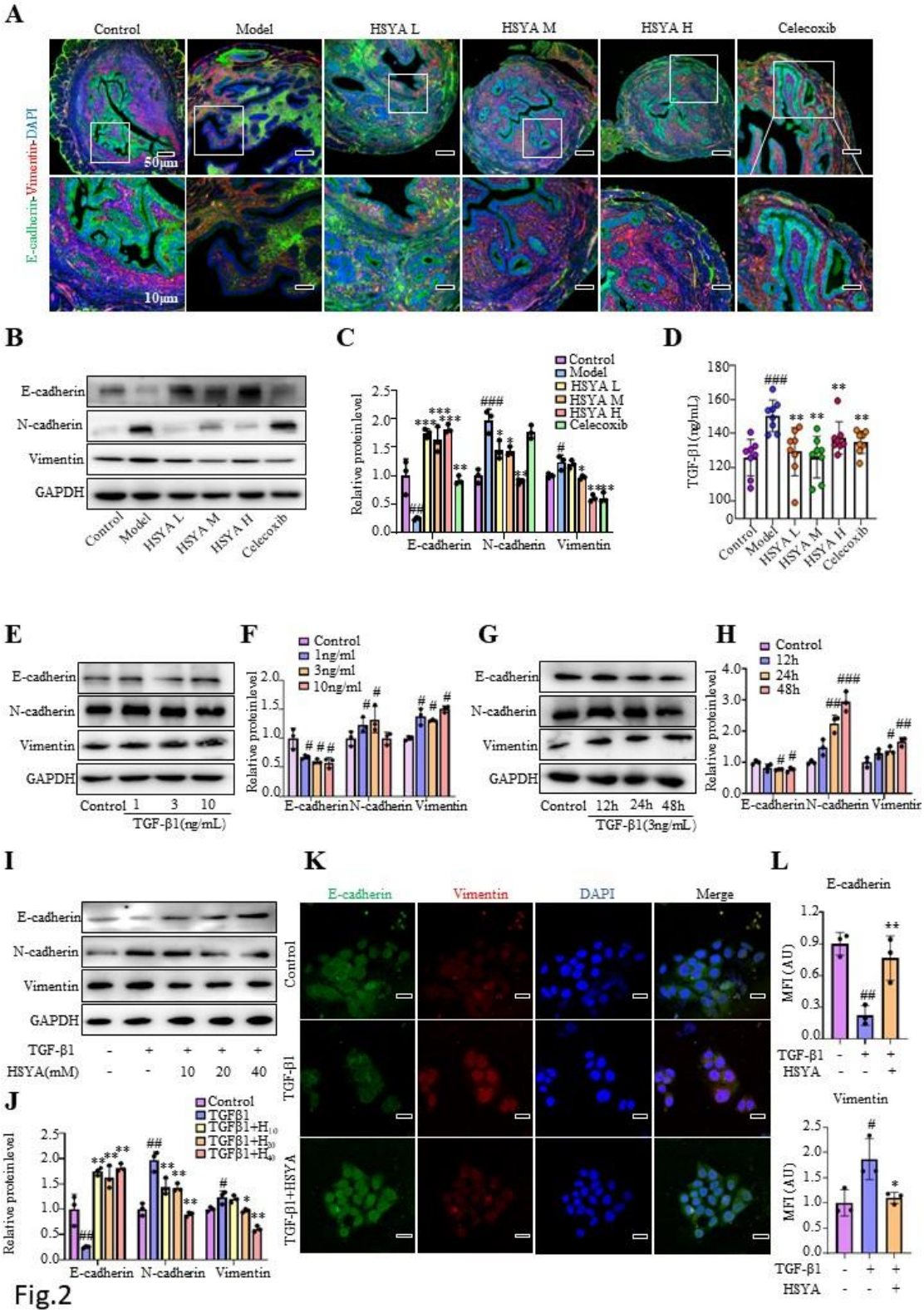
A
Control
Model
HSYA L
HSYA M
HSYA H
Celecoxib
E-cadherin-Vimentin-DAPI
50μm
10μm
B
E-cadherin
N-cadherin
Vimentin
GAPDH
C
Control
Model
HSYA L
HSYA M
HSYA H
Celecoxib
Relative protein level
D
TGF-β1 (ng/mL)
E
TGF-β1(ng/mL)
F
1ng/ml
3ng/ml
10ng/ml
G
TGF-β1(3ng/mL)
H
12h
24h
48h
I
TGF-β1
HSYA(mM)
J
TGFβ1
TGFβ1+H10
TGFβ1+H30
TGFβ1+H40
K
E-cadherin
Vimentin
DAPI
Merge
TGF-β1
TGF-β1+HSYA
L
MFI (AU)

Fig.2

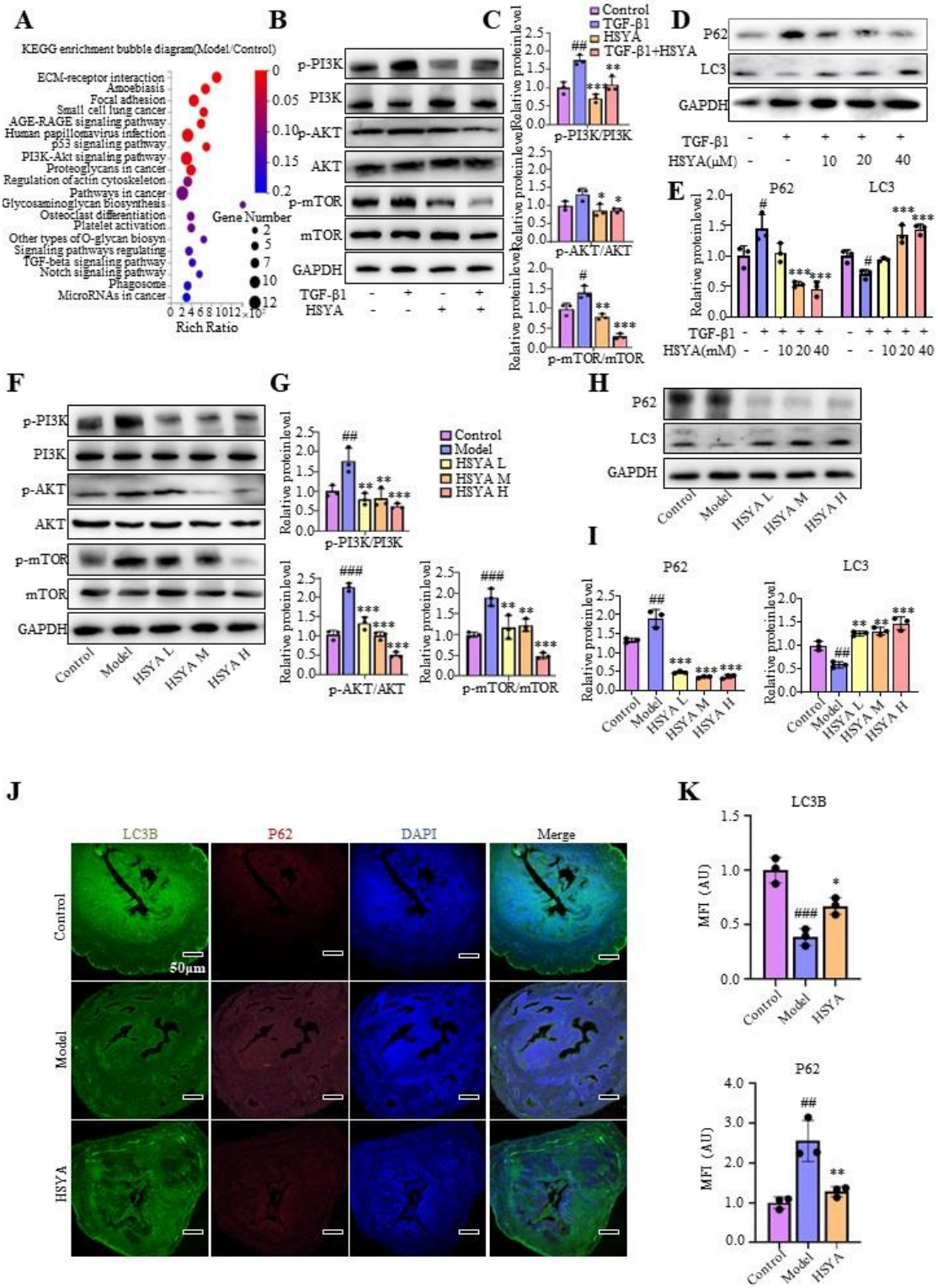
A
KEGG enrichment bubble diagram(Model/Control)
ECM-receptor interaction
Amoebiasis
Focal adhesion
Small cell lung cancer
AGE-RAGE signaling pathway
Human papillomavirus infection
p53 signaling pathway
PI3K-Akt signaling pathway
Proteoglycans in cancer
Regulation of actin cytoskeleton
Pathways in cancer
Glycosaminoglycan biosynthesis
Osteoclast differentiation
Platelet activation
Other types of O-glycan biosyn
Signaling pathways regulating
TGF-beta signaling pathway
Notch signaling pathway
Phagosome
MicroRNAs in cancer
Rich Ratio
Gene Number
B
p-PI3K
PI3K
p-AKT
AKT
p-mTOR
mTOR
GAPDH
TGF-β1
HSYA
C
Control
TGF-β1
HSYA
TGF-β1+HSYA
Relative protein level
p-PI3K/PI3K
p-AKT/AKT
p-mTOR/mTOR
D
P62
LC3
GAPDH
TGF-β1
HSYA(μM)
E
P62
LC3
Relative protein level
TGF-β1
HSYA(mM)
F
p-PI3K
PI3K
p-AKT
AKT
p-mTOR
mTOR
GAPDH
Control
Model
HSYA L
HSYA M
HSYA H
G
Control
Model
HSYA L
HSYA M
HSYA H
Relative protein level
p-PI3K/PI3K
p-AKT/AKT
p-mTOR/mTOR
H
P62
LC3
GAPDH
I
P62
LC3
Relative protein level
J
LC3B
P62
DAPI
Merge
Control
Model
HSYA
50μm
K
LC3B
MFI (AU)
P62
MFI (AU)

Fig.3

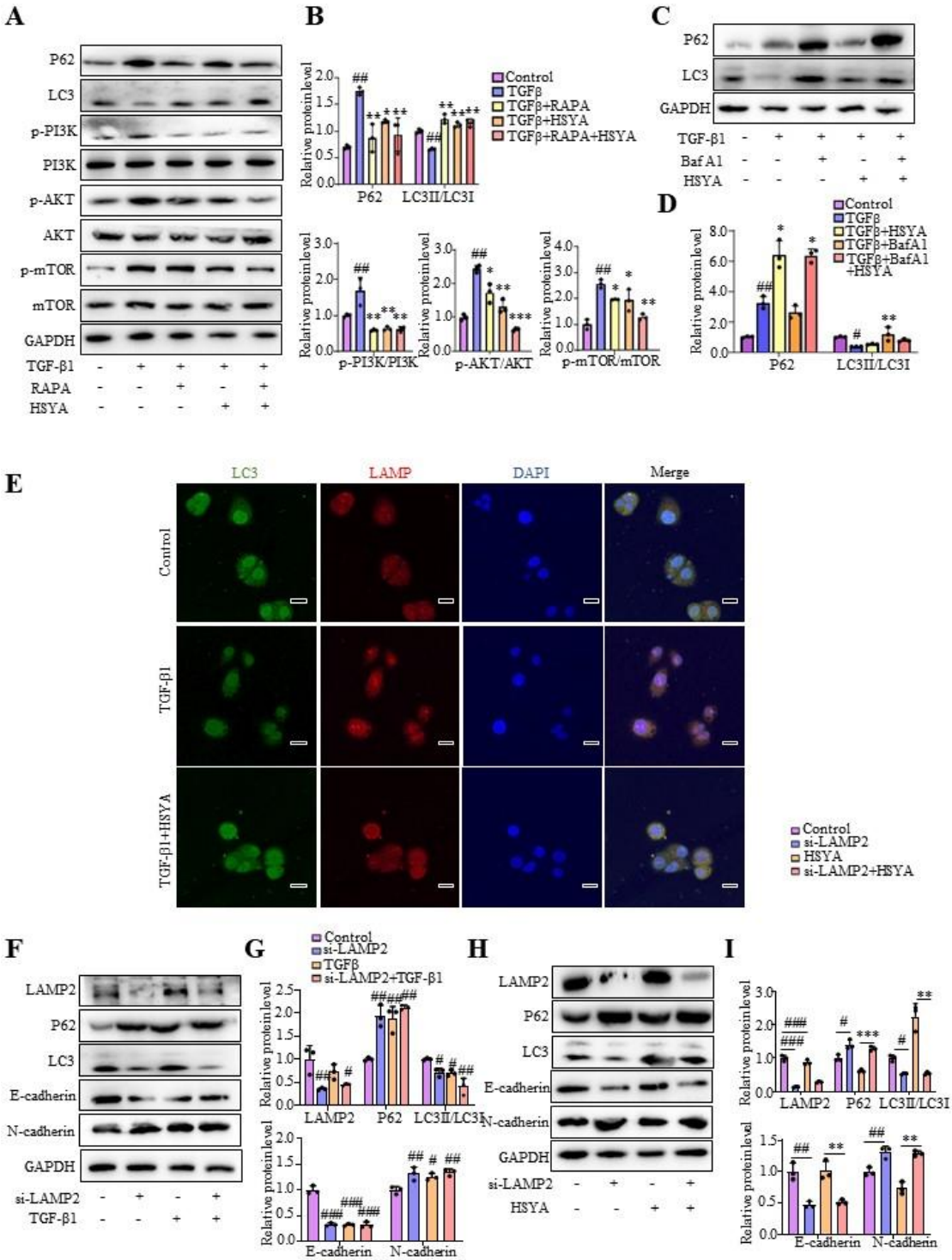
A
P62
LC3
p-PI3K
PI3K
p-AKT
AKT
p-mTOR
mTOR
GAPDH
TGF-β1
RAPA
HSYA
B
Control
TGFβ
TGFβ+RAPA
TGFβ+HSYA
TGFβ+RAPA+HSYA
Relative protein level
P62
LC3II/LC3I
p-PI3K/PI3K
p-AKT/AKT
p-mTOR/mTOR
C
P62
LC3
GAPDH
TGF-β1
Baf A1
HSYA
D
Control
TGFβ
TGFβ+HSYA
TGFβ+BafA1
TGFβ+BafA1 +HSYA
Relative protein level
P62
LC3II/LC3I
E
LC3
LAMP
DAPI
Merge
Control
TGF-β1
TGF-β1+HSYA
Control
si-LAMP2
HSYA
si-LAMP2+HSYA
F
LAMP2
P62
LC3
E-cadherin
N-cadherin
GAPDH
si-LAMP2
TGF-β1
G
Control
si-LAMP2
TGFβ
si-LAMP2+TGF-β1
Relative protein level
LAMP2
P62
LC3II/LC3I
E-cadherin
N-cadherin
H
LAMP2
P62
LC3
E-cadherin
N-cadherin
GAPDH
si-LAMP2
HSYA
I
Relative protein level
LAMP2
P62
LC3II/LC3I
E-cadherin
N-cadherin

Fig.4

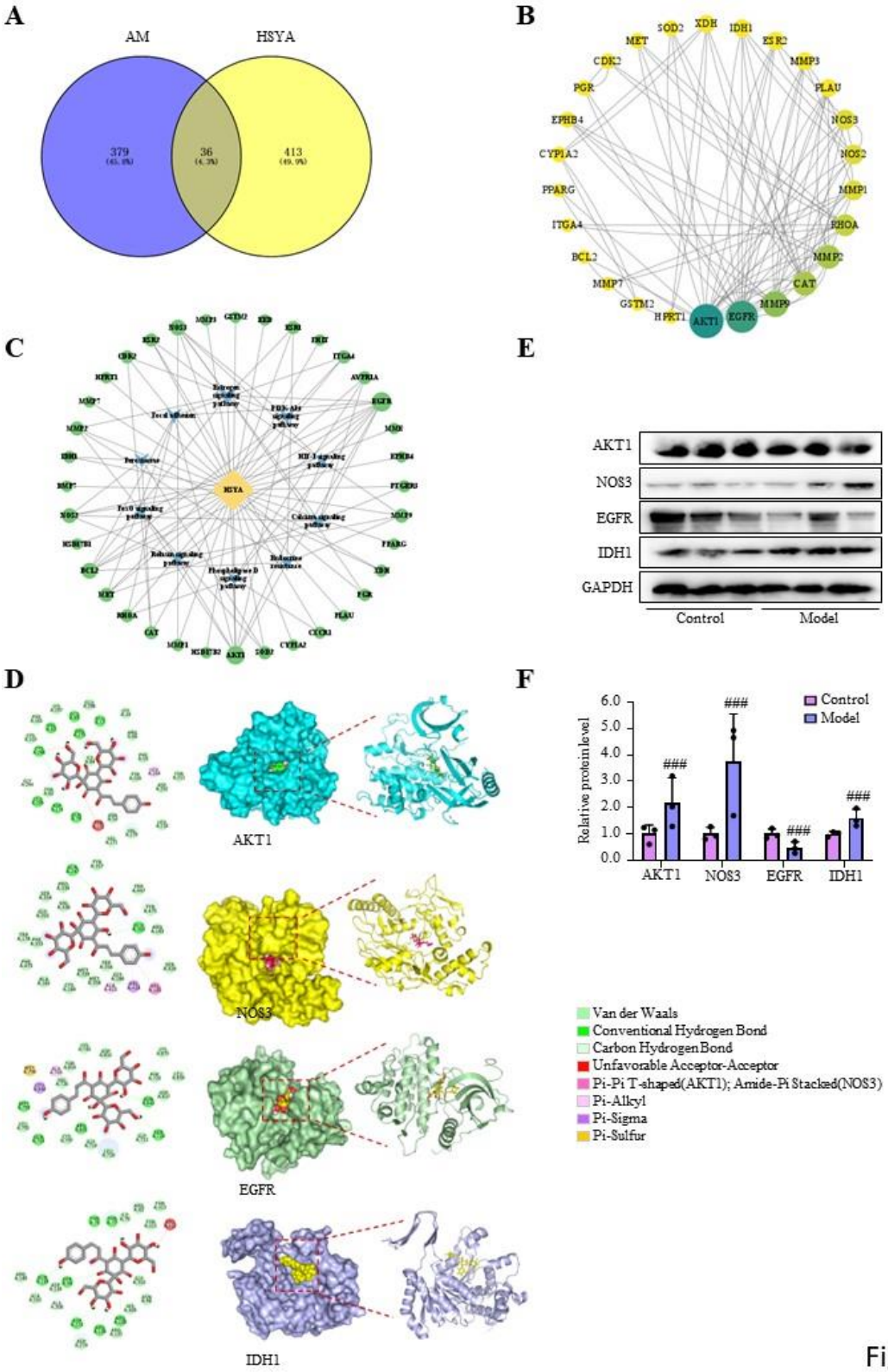
A
AM
HSYA
379
(91.8%)
36
(8.3%)
413
(49.9%)
B
SOD2
XDH
IDH1
MET
ESR2
CDK2
MMP3
PGR
PLAU
EPHB4
NOS3
CYP1A2
NOS2
PPARG
MMP1
ITGA4
RHOA
BCL2
MMP2
MMP7
CAT
GSTM2
MMP9
HPRT1
AKT1
EGFR
C
HSYA
E
AKT1
NOS3
EGFR
IDH1
GAPDH
Control
Model
D
AKT1
NOS3
EGFR
IDH1
F
Relative protein level
Control
Model
###
AKT1
NOS3
EGFR
IDH1
Van der Waals
Conventional Hydrogen Bond
Carbon Hydrogen Bond
Unfavorable Acceptor-Acceptor
Pi-Pi T-shaped(AKT1); Amide-Pi Stacked(NOS3)
Pi-Alkyl
Pi-Sigma
Pi-Sulfur

Fig.5

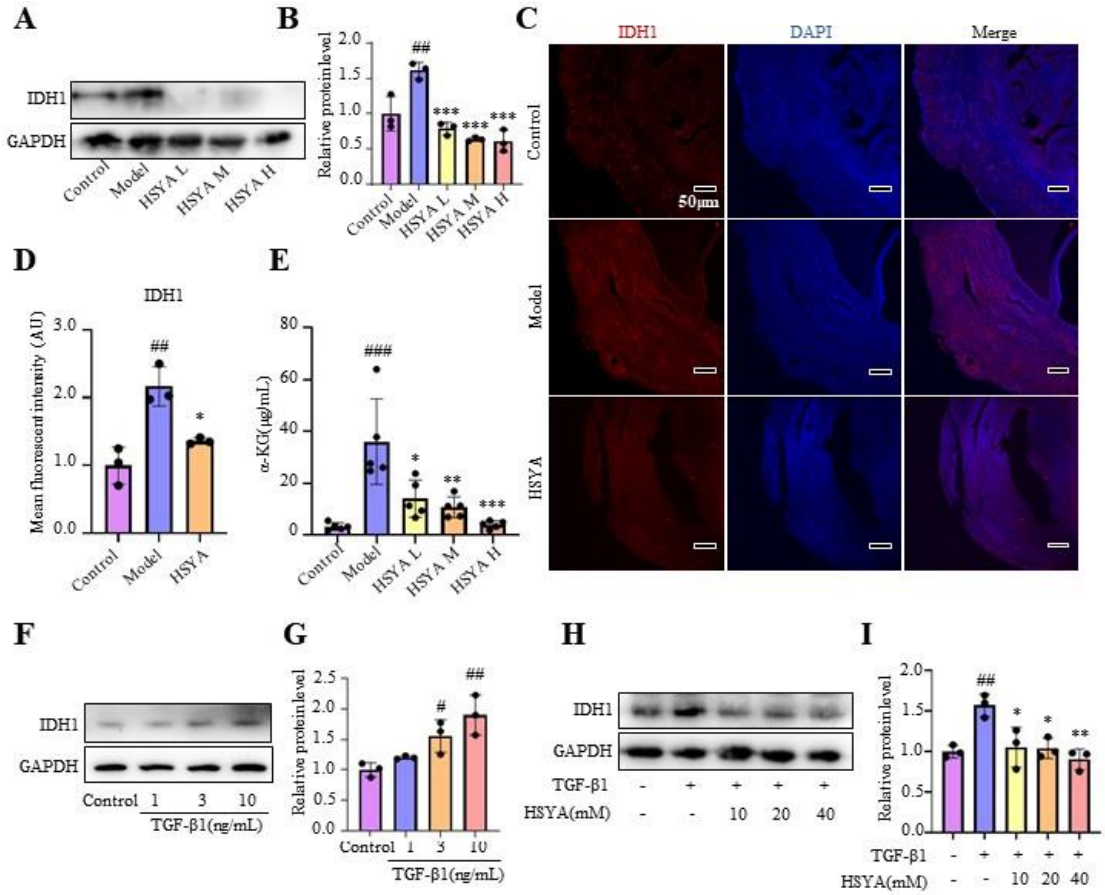
A
IDH1
GAPDH
Control
Model
HSYA L
HSYA M
HSYA H
B
Relative protein level
C
IDH1
DAPI
Merge
Control
Model
HSYA
50μm
D
IDH1
Mean fluorescent intensity (AU)
E
α-KG(μg/mL)
F
IDH1
GAPDH
Control 1 3 10
TGF-β1(ng/mL)
G
Relative protein level
H
IDH1
GAPDH
TGF-β1
HSYA(mM)
I
Relative protein level
TGF-β1
HSYA(mM)

Fig.6

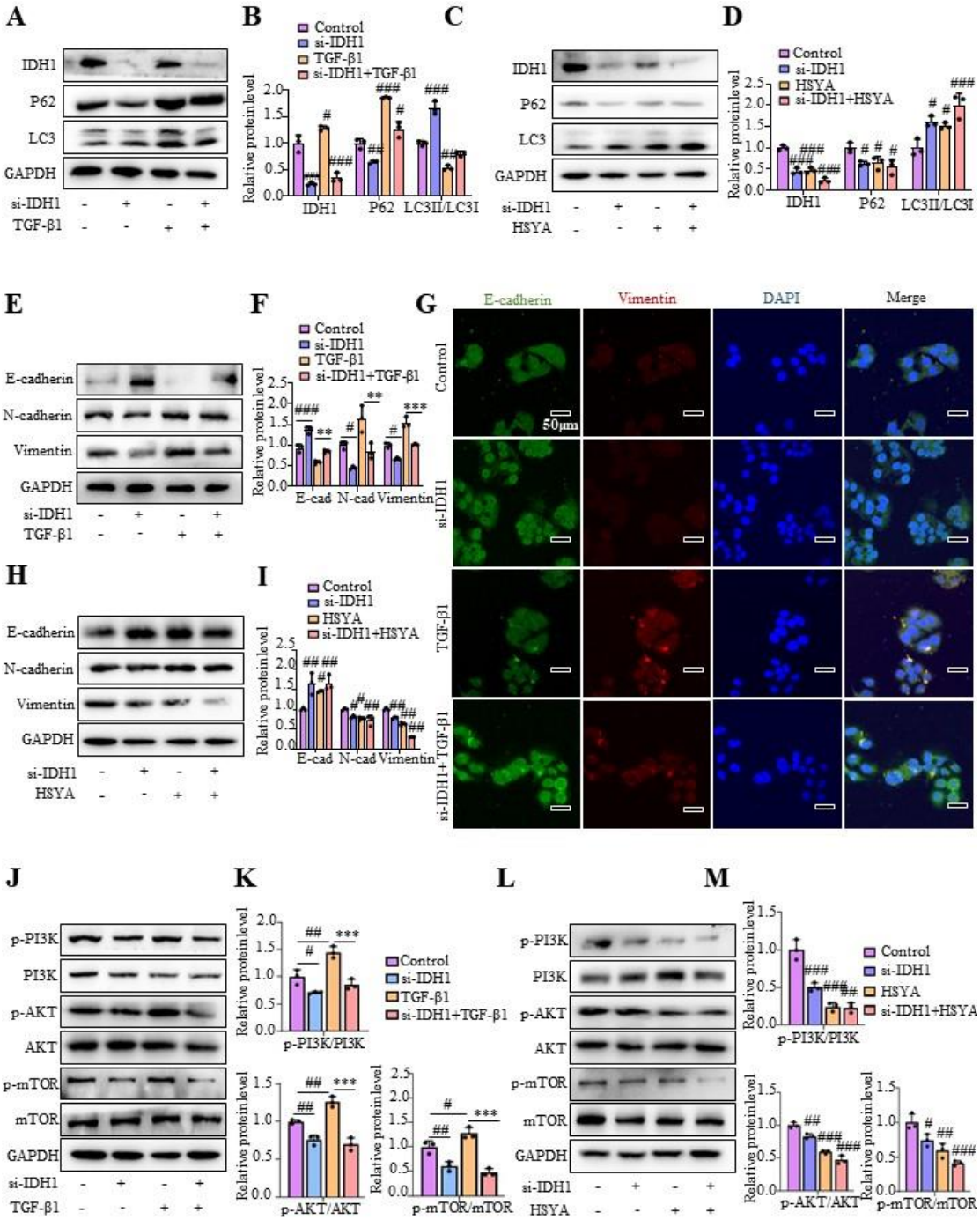
A
IDH1
P62
LC3
GAPDH
si-IDH1
TGF-β1
B
Control
si-IDH1
TGF-β1
si-IDH1+TGF-β1
Relative protein level
IDH1
P62
LC3II/LC3I
C
HSYA
si-IDH1+HSYA
D
E
E-cadherin
N-cadherin
Vimentin
F
E-cad
N-cad
G
E-cadherin
Vimentin
DAPI
Merge
Control
50μm
H
I
J
p-PI3K
PI3K
p-AKT
AKT
p-mTOR
mTOR
K
p-PI3K/PI3K
p-AKT/AKT
p-mTOR/mTOR
L
M

Fig.7

Legends

Figure 1. HSYA attenuated Tamoxifen-induced mice adenomyosis. A. Chemical structure of HSYA. B. Experimental design in vivo. C. Representative images of the uteri, H&E staining and Masson's trichrome staining of mice uteri. D. Grade quantification of myometrial infiltration in the endometrium. E. Quantification of Masson's trichrome staining. Data were represented as mean ± SEM. $^{\#}p < 0.05$, $^{\#\#}p < 0.01$, $^{\#\#\#}p<0.001$ vs Control. $^{*}p < 0.05$, $^{**}p < 0.01$ vs Model.

Figure 2. HSYA inhibited EMT of adenomyosis mice. A. Representative immunofluorescence images of Vimentin (red), E-cadherin (green) and DAPI nuclear stains (blue) in paraffin section of mice uteri. B. Western blots of E-cadherin, N-cadherin and Vimentin in mouse uteri. C. Quantification of Fig.2B. D. TGF-β1 in the serum was determined by ELISA. E. Western blots of E-cadherin, N-cadherin and Vimentin in Ishikawa cells treated with TGF-β1 (0, 1, 3, 10 ng/mL) for the indicated concentration. F. Quantification of Fig.2D. G. Western blots of E-cadherin, N-cadherin and Vimentin in Ishikawa cells treated in the absence or presence of TGF-β1 (3 ng/mL) for the indicated time. H. Quantification of Fig.2G. I. Western blots of E-cadherin, N-cadherin, Vimentin in Ishikawa cells treated with HSYA (10, 20, 40 μM) for 24h in the absence or presence of TGF-β1 (3 ng/mL). J. Quantification of Fig.2I. K. Representative immunofluorescence images of Vimentin(red), E-cadherin(green) and DAPI nuclear stains (blue) in Ishikawa cells. L. Quantification of Fig.2K. Data were shown as means ± SEM. $^{\#}p < 0.05$, $^{\#\#}p < 0.01$, $^{\#\#\#}p<0.001$vs Control. $^{*}p < 0.05$, $^{**}p < 0.01$, $^{***}p<0.001$ vs Model.

Figure 3. HSYA induced autophagic flux via PI3K-Akt signaling pathway in Ishikawa cells and adenomyosis mice. A. Scatterplot of enriched KEGG pathways analyzed by transcriptome of Ishikawa cells treated with or without TGF-β1 (3 ng/mL). B. Western blots of p-PI3K, PI3K, p-AKT, AKT, p-mTOR and mTOR in Ishikawa cells treated with or without HSYA (40 μM) for 24 h in the absence or presence of TGF-β1 (3 ng/mL). C. Quantification of Fig.3B. D. Western blots of p62 and LC3 in Ishikawa cells treated with or without HSYA (10, 20 and 40 μM) for 24h in the absence or presence of TGF-β1 (3 ng/mL). E. Quantification of Fig.3D. F. Western blots of p-PI3K, PI3K, p-AKT, AKT, p-mTOR, and mTOR in the uterus of adenomyosis mice. G. Quantification of Fig.3F. H. Western blots of p62 and LC3 in Ishikawa cells treated with or without HSYA (10, 20 and 40 μM) for 24h in the absence or presence of TGF-β1 (3 ng/mL). I. Quantification of Fig.3H. J. Representative immunofluorescence images of P62 (red), LC3(green) and DAPI nuclear stains (blue) in paraffin section of mice uterus. K. Quantification of Fig.3J. Data were shown as means ± SEM. $^{\#}p < 0.05$, $^{\#\#}p < 0.01$, $^{\#\#\#}p<0.001$ vs Control. $^{*}p < 0.05$, $^{**}p < 0.01$, $^{***}p<0.001$ vs Model.

Figure 4. HSYA induced autophagic flux and improved EMT through PI3K-Akt

signaling pathway in Ishikawa cells. A. Western blots of P62, LC3, p-PI3K, PI3K, p-AKT, AKT, p-mTOR, mTOR in Ishikawa cells treated with or without HSYA (10, 20 μM) in the absence or presence of TGF-β1 (3 ng/mL) or Rapamycin (100 nM) for 24h. B. Quantification of Fig.4A. C. Western blots of P62 and LC3 in Ishikawa cells treated with or without HSYA (40μM) in the absence or presence of TGF-β1 (3 ng/mL) or Baf A1 (200 nM) for 24h. D. Quantification of Fig.4C. E. Representative immunofluorescence images of LAMP (red), LC3 (green) and DAPI nuclear stains (blue) in Ishikawa cells treated with HSYA (40 μM) in the presence or absence of TGF-β1 (3 ng/mL). F. Western blots of LAMP, P62, LC3, E-cadherin, and N-cadherin in Ishikawa cells transfected with or without LAMP siRNA in the presence or absence of TGF-β1 (3 ng/mL) for 24h. G. Quantification of Fig.4F. H. Western blots of LAMP, P62, LC3, E-cadherin and N-cadherin in Ishikawa cells transfected with or without LAMP siRNA in the presence or absence of HSYA (40μM) for 24h. I. Quantification of Fig.4H. Data were represented as means ± SEM. $^{\#}p < 0.05$, $^{\#\#}p < 0.01$, $^{\#\#\#}p<0.001$ vs Control. $^{*}p < 0.05$, $^{**}p < 0.01$, $^{***}p<0.001$ vs Model.

Figure 5. Identification and docking verification of HSYA Core Targets against adenomyosis. A. Venn diagram of potential targets of HSYA for adenomyosis treatment. B. Visualizing PPI network via Cytoscape 3.7.1 software. The color and size of the node represented the Degree value, which the darker color and the larger size of the node implied a greater Degree value. C. Component-target-pathway network analysis. HSYA, the potential core targets, and the ten disease-related pathways were shown. D. Molecular docking analysis of potential core targets with HSYA. E. Western blots of AKT1, NOS3, EGFR and IDH1 in mouse and human uterine tissue. F. Quantification of Fig.5E. Data were shown as means ± SEM. $^{\#\#\#}p<0.001$ vs Control.

Figure 6. HSYA attenuated IHD1 in adenomyosis mice and Ishikawa cells. A. Western blots of IDH1 in adenomyosis mouse uterine. B. Quantification of Fig.6A. C. Representative immunofluorescence images of paraffin section of mice uterus. IDH1 stains (red) and DAPI nuclear stains (blue). D. Quantification of Fig.6C. E. ELISA analysis of α-KG in mice uterus. F. Western blots of IDH1 in ishikawa cells treated with TGFβ1(0, 1, 3, 10 ng/Ml) for 24h. G. Quantification of Fig.6E. H. Western blots of IDH1 in Ishikawa cells treated with HSYA (0, 10, 20, 40 μM) for 24h in the absence or presence of TGFβ1 (3 ng/mL). I. Quantification of Fig.6H. Data were represented as means ± SEM. $^{\#}p < 0.05$, $^{\#\#}p < 0.01$, $^{\#\#\#}p<0.001$ vs Control. $^{*}p < 0.05$, $^{**}p < 0.01$, $^{***}p<0.001$ vs Model.

Figure 7. HSYA attenuated IHD1 and enhanced autophagy. A. Western blots of IDH1, P62 and LC3 in Ishikawa cells treated with or without TGFβ1 (3 ng/mL) in the absence or presence of si-IDH1. B. Quantification of Fig.7A. C. Western blots of IDH1, P62 and LC3 in Ishikawa cells treated with HSYA (40 μM). D. Quantification of Fig.7C. E. Western blots of E-cadherin, N-cadherin and Vimentin in Ishikawa cells treated with or without TGFβ1 (3 ng/mL) in the absence or presence of si-IDH1. F. Quantification of Fig.7E. G. Representative immunofluorescence images of E-cadherin (green),

Vimentin (red) and DAPI nuclear stains (blue) in Ishikawa cells treated with or without TGFβ1 (3 ng/mL) in the presence or absence of si-IDH1. H. Western blots of E-cadherin, N-cadherin and Vimentin in Ishikawa cells treated with or without HSYA (40μM) in the absence or presence of si-IDH1. I. Quantification of Fig.7H. J. Western blots of p-PI3K, PI3K, p-AKT, AKT, p-mTOR, and mTOR in Ishikawa cells treated with or without TGFβ1 (3 ng/mL) in the absence or presence of si-IDH1. K. Quantification of Fig.7J. L. Western blots of p-PI3K, PI3K, p-AKT, AKT, p-mTOR, and mTOR in Ishikawa cells treated with or without HSYA (40 μM) in the absence or presence of si-IDH1. M. Quantification of Fig.7L. Data were shown as means ± SEM. $^{\#}p < 0.05$, $^{\#\#}p < 0.01$, $^{\#\#\#}p<0.001$ vs Control. *p < 0.05, **p < 0.01, ***p<0.001 vs Model.